

# Free-carrier and phonon properties of *n*- and *p*-type hexagonal GaN films measured by infrared ellipsometry

A. Kasic and M. Schubert\*

*Center for Microelectronic and Optical Materials Research, University of Nebraska, Lincoln, Nebraska, 68588*

S. Einfeldt and D. Hommel

*Institut für Festkörperphysik, Universität Bremen, 28359 Bremen, Germany*

T. E. Tiwald

*J. A. Woollam Co., 645 M Street, Suite 102, Lincoln, Nebraska 68508*

(Received 28 December 1999; revised manuscript received 10 May 2000)

Infrared spectroscopic ellipsometry (IRSE) over the wave-number range from 300 to 1200  $\text{cm}^{-1}$  is used to determine the anisotropic room-temperature optical properties of highly resistive, Si-doped *n*-type and Mg-doped *p*-type  $\alpha$ -GaN. The approximately 1- $\mu\text{m}$ -thick films were deposited on *c*-plane sapphire by molecular beam epitaxy without a buffer layer. The free-carrier concentrations are obtained from Hall measurements. The IRSE data are analyzed through model calculations of the infrared optical dielectric functions parallel ( $\parallel$ ) and perpendicular ( $\perp$ ) to the *c* axis of the  $\alpha$ -GaN films. We obtain the thin-film phonon frequencies and broadening values and the optical mobility and effective-mass parameters for *n*- and *p*-type  $\alpha$ -GaN. In agreement with Perlin *et al.* [Appl. Phys. Lett. **68**, 1114 (1996)] we determine the effective electron masses as  $m_{e,\perp}/m_0 = 0.237 \pm 0.006$  and  $m_{e,\parallel}/m_0 = 0.228 \pm 0.008$ . For *p*-type GaN with hole concentration  $N_h = 8 \times 10^{17} \text{cm}^{-3}$  we find  $m_h/m_0 = 1.40 \pm 0.33$ , which agrees with recent theoretical studies of the Rashba-Sheka-Pikus parameters in wurtzite GaN. However, no substantial anisotropy of the effective hole mass is obtained to within 25%. The ellipsometry data also allow for derivation of the model quantities  $\epsilon_{\infty,j}$  ( $j = \perp, \parallel$ ), which are almost isotropic but may vary between 4.92 and 5.37 depending on whether the films are undoped or doped. In heavily-Si-doped *n*-type  $\alpha$ -GaN we observe a thin carrier-depleted surface layer and additional infrared-active vibrational modes at 574, 746, and 851  $\text{cm}^{-1}$ . Raman measurements of the GaN films are also performed, and the results are compared to those obtained from the IRSE investigations.

## I. INTRODUCTION

Recent enormous progress in the development and design of group-III nitride optoelectronic devices operating in the blue and near-ultraviolet wavelength region demands better understanding of the optical properties of GaN and its related compounds.<sup>1-3</sup> The optical response of materials in the infrared (ir) spectral region is of high interest because phonon modes and their coupling behavior reflect physical properties of crystals such as the lattice symmetry and quality and internal stress, as well as free-carrier parameters.<sup>4</sup> Wurtzite-type GaN ( $\alpha$ -GaN) is expected to possess strong anisotropy of the valence-band mass parameters.<sup>3,5-8</sup> Effective electron and hole masses and their anisotropy are crucial parameters for design and understanding of device structures.<sup>9,10</sup> Likewise, nondestructive measurement of free-carrier mobility parameters in complex heterostructures remains a challenge.

Raman, as well as ir-reflectometry (reflection and also transmission spectroscopy) techniques are widely used to characterize the ir optical properties of GaN film and bulk material.<sup>3</sup> Influence of strain,<sup>11</sup> substrate materials,<sup>12</sup> and growth orientations<sup>12,13</sup> have been studied. The coupling of longitudinal-optical (LO) phonons with free-carrier plasmon excitations [LO-phonon-plasmon (LPP) modes] has been observed and studied in *n*-type material.<sup>14-20</sup> Barker and Ilegems<sup>14</sup> used ir reflectometry and reported the phonon modes for wurtzite ( $\alpha$ -GaN) films. The high-frequency di-

electric constant values were set to  $\epsilon_{\infty,\perp} = \epsilon_{\infty,\parallel} = 5.35$ .<sup>14</sup> They also provided the effective electron mass  $m_{e,\perp}/m_0 = 0.20 \pm 0.02$ , which was found to be isotropic to within 30%. Perlin *et al.*<sup>15</sup> fitted ir-reflectometry data of  $\alpha$ -GaN bulk crystals and obtained  $m_e/m_0 = 0.22 \pm 0.02$  without significant anisotropy but assumed  $\epsilon_{\infty,\perp} = \epsilon_{\infty,\parallel} = 5.2$ .<sup>21</sup> The effective electron mass values determined by Barker and Ilegems<sup>14</sup> and Perlin *et al.*<sup>15</sup> using ir reflectometry are now commonly adopted for *n*-type  $\alpha$ -GaN. Reports on Raman observation of free-carrier effects in *p*-type  $\alpha$ -GaN are still rare,<sup>22-24</sup> and, to the best of our knowledge, no ir-reflectometry experiment to obtain the effective mass from *p*-conductive  $\alpha$ -GaN films has been reported so far. Popovici *et al.*<sup>22</sup> performed Raman scattering on *p*-type GaN films with free-hole concentration  $N_h = (2-7) \times 10^{17} \text{cm}^{-3}$ , but did not observe LPP coupling. The authors concluded that it may in general be difficult to observe *p*-type LPP modes because of the larger effective hole mass ( $m_h = 0.8m_0$  was assumed) and the lower maximum hole concentration available compared to the case of electrons. Furthermore, hole plasmons are more strongly damped than electron plasmons due to the typically very low hole-mobility values [ $\mu_h \leq 20 \text{cm}^2/(\text{Vs})$ ]. Demangeot *et al.*<sup>23</sup> studied Raman scattering in *p*-type  $\alpha$ -GaN films with hole concentrations of up to  $3 \times 10^{18} \text{cm}^{-3}$ . The lattice LO-mode frequencies were slightly shifted by the nonresonant free-hole gas. The effective-hole-mass value of  $0.8m_0$  from Ref.

25 and carrier concentrations and mobilities from Hall measurements were assumed for line-shape analysis of the weakly coupled LPP modes. Evidence for hole-mass anisotropy was claimed from a weak discrepancy between calculated and measured  $A_1$  LPP modes. However, Popovici *et al.*<sup>22</sup> as well as Harima *et al.*<sup>24</sup> concluded from their Raman studies that precise evaluation of  $p$ -type electrical transport parameters in  $\alpha$ -GaN, such as carrier density and mobility, from LPP-mode profiles alone is difficult.

Attempts to estimate the effective hole masses and their anisotropy in  $\alpha$ -GaN have been made from analysis of absorption and luminescence experiments. Kosicki *et al.*<sup>26</sup> estimated from near-band-gap absorption coefficients  $m_h/m_0 \geq 0.6$ , but assumed cubic symmetry and parabolic valence bands. Cunningham *et al.*<sup>27</sup> chose  $m_h/m_0 = 1.0$  to reasonably fit luminescence band-to-band transition energies to the Burstein shift in  $n$ -type  $\alpha$ -GaN. More recently, Merz *et al.*<sup>28</sup> calculated the isotropically averaged heavy-hole (hh) mass  $m_{hh}/m_0 \approx 0.54$  from luminescence data. A considerably higher value for the lower bound of the effective hole mass,  $m_h/m_0 \approx 2.2 \pm 0.2$ , was determined by Im *et al.*<sup>29</sup> from analysis of the interband transition matrix element obtained from time-resolved photoluminescence experiments and absorption data. They assumed that the effective masses of the two uppermost valence bands are the same. Using two-photon spectroscopy, Steube *et al.*<sup>30</sup> observed the  $2P$  excitons associated with the heavy-hole, light-hole (lh), and split-off-hole (sh) uppermost valence-band states in  $\alpha$ -GaN, and derived isotropic effective hole masses  $m_{hh}/m_0 = 1.0 \pm 0.1$ ,  $m_{lh}/m_0 = 1.1 \pm 0.2$ , and  $m_{sh}/m_0 = 1.6 \pm 0.5$  under the assumption of hydrogenlike exciton series.

Theoretical investigations of the electronic properties of  $\alpha$ -GaN have been performed by several methods.<sup>5–8</sup> Suzuki *et al.*<sup>5</sup> employed a self-consistent full-potential linearized augmented plane-wave method within the local-density-functional approximation and presented their results within the effective-mass approximation. Small anisotropy was found for the conduction-band masses ( $m_{e,\parallel}/m_0 = 0.20$ ,  $m_{e,\perp}/m_0 = 0.18$ ). Strong anisotropy was obtained for the effective hole masses ( $m_{hh,\parallel}/m_0 = 1.76$ ,  $m_{hh,\perp}/m_0 = 1.61$ ,  $m_{lh,\parallel}/m_0 = 1.76$ ,  $m_{lh,\perp}/m_0 = 0.14$ ,  $m_{sh,\parallel}/m_0 = 0.16$ ,  $m_{sh,\perp}/m_0 = 1.04$ ). Kim *et al.*<sup>7</sup> used full-potential linearized muffin-tin orbital calculation to study the conduction- and valence-band effective-mass tensors, and the related Rashba-Sheka-Pikus parameters for  $\alpha$ -GaN. Conduction-band masses are in very good agreement with the generally accepted values, and valence-band mass parameters are  $m_{hh,\parallel}/m_0 = 2.00$ ,  $m_{hh,\perp}/m_0 = 0.33$ ,  $m_{lh,\parallel}/m_0 = 1.17$ ,  $m_{lh,\perp}/m_0 = 0.35$ ,  $m_{sh,\parallel}/m_0 = 0.15$ ,  $m_{sh,\perp}/m_0 = 1.53$ , with a much smaller  $m_{hh,\perp}$  value than obtained in Ref. 5. Chen *et al.*<sup>6</sup> reported similar results from first-principles band-structure calculations. Kim *et al.*<sup>7</sup> also calculated the energy-dependent effective hole masses, suggesting strong changes of the effective masses for hole Fermi levels within the valence bands. In particular, the small  $m_{hh,\perp}$  value rapidly approaches  $\sim 1.75m_0$  for hole energies of  $\sim 25$  meV, and measurements of effective hole parameters in  $p$ -type  $\alpha$ -GaN films will likely depend on the actual hole concentration.

The influence of the carrier concentration on the LPP-mode Raman signals or ir reflectivity usually permits the determination of the free-carrier concentration if the

effective-mass parameters and the high-frequency dielectric constants are known.<sup>4,31</sup> Likewise, if the carrier concentration is known from Hall measurements, mobility and effective-mass parameters can be calculated from the ir dielectric response.<sup>14,15</sup> But so far, Raman scattering and ir-reflectometry techniques failed to measure free-carrier quantities in  $p$ -type  $\alpha$ -GaN mostly because of (i) the weak LPP coupling<sup>22,24</sup> and (ii) the insensitivity of ir-reflectometry data to small changes in thin-film optical properties.<sup>32</sup> Spectroscopic ellipsometry (SE) can overcome both problems as will be shown in this article. SE is known as an excellent technique for determination of the complex dielectric function  $\epsilon$  of thin-film materials.<sup>32</sup> Recent development of polarization-sensitive spectrophotometers in the mid- and far-ir enable the application of SE for wavelengths that match the phonon frequencies of many III-V semiconducting compounds.<sup>33–37</sup> Because SE determines both real and imaginary parts of  $\epsilon$  simultaneously, inaccuracies due to extrapolation into experimentally inaccessible spectral regions, as necessary for Kramers-Kronig analysis to obtain this information from ir-reflectivity data, are avoided.<sup>32</sup> The analysis of the ellipsometric data in the far- and mid-ir spectral range for anisotropic multilayered systems with plane-parallel interfaces requires the same matrix algorithm and nonlinear regression approaches as widely used for the visible and near-ir spectral range.<sup>38–42</sup> SE as well as ir-reflectometry is an indirect technique for dielectric function determination because the calculated data must be fitted to the measured data by varying the model parameters under appropriate physical assumptions for the spectral dependence of  $\epsilon$ .<sup>38–41</sup> A factorized model was used recently for successful parametrization of the anisotropic infrared dielectric functions of  $\alpha$ -sapphire.<sup>43</sup> This model descended from consideration of anharmonic lattice response effects and contains independent broadening values for each transversal-optical (TO) and LO lattice mode. The different broadening parameters account for different decay mechanisms for the TO- and LO-phonon of the same branch. Based on coupled-optical-phonon-mode theory presented by Barker and Hopfield,<sup>44</sup> introduced by Berreman and Unterwald,<sup>45</sup> and further theorized by Gervais and Piriou,<sup>46</sup> Kukharskii<sup>47</sup> included effects of plasmons into this factorized form of the long-wavelength dielectric function model. Kukharskii's extended model thus allows for anharmonic coupling of LO phonons with free-carrier plasmon excitations.<sup>47</sup> Humlíček once criticized the use of the anharmonic factorized form.<sup>48</sup> He found that the factorized form of Gervais and Piriou produces dielectric functions for  $\alpha$ -quartz that differed substantially from those obtained by him using ellipsometric data and sums of harmonic Lorentz oscillator terms.<sup>45,46</sup> On the other hand, in a recent publication Humlíček, Henn, and Cardona<sup>49</sup> use the “ $K$ -mode” dielectric function of Barker and Hopfield,<sup>44</sup> which is essentially equivalent to the factorized form of Gervais and Piriou, in order to model the dielectric response of uniaxial LaSrGaO<sub>4</sub> and LaSrAlO<sub>4</sub> considering anharmonic lattice effects. Recently, Schubert, Tiwald, and Herzinger also preferred the factorized model and not the harmonic Lorentz sum model in order to accurately describe the anisotropic dielectric functions for sapphire.<sup>43</sup>

This work reports on infrared spectroscopic ellipsometry

(IRSE) measurement of the anisotropic dielectric response of highly resistive,  $n$ -type, and  $p$ -type  $\alpha$ -GaN. The GaN free-carrier concentrations are obtained from Hall measurements. Using the Hall data, we derive the free-carrier mobilities and effective masses, as well as the phonon frequencies and broadening values and the high-frequency dielectric constants for highly doped  $n$ - and  $p$ -type  $\alpha$ -GaN. For highly resistive  $\alpha$ -GaN the IRSE data are still sensitive to free-carrier concentrations in the range of  $\sim 8 \times 10^{16} \text{ cm}^{-3}$ , which were obtained assuming the effective electron mass value of Ref. 15. We determine the frequencies of the  $E_1(\text{TO})$ ,  $A_1(\text{LO})$ , and  $E_1(\text{LO})$   $\alpha$ -GaN lattice modes, the  $E_1(\text{TO})$  and LPP-mode broadening values, and the anisotropic LPP-mode and plasma frequencies. The layer thickness is also obtained precisely. We further observe additional ir-active impurity-like vibrational modes in highly-Si-doped  $\alpha$ -GaN, which occur within the  $\alpha$ -GaN reststrahlen band. We also find a thin carrier-depleted surface layer in the highly-Si-doped sample.

## II. THEORY

### A. GaN phonon modes

The crystalline structure of wurtzite-type GaN ( $\alpha$ -GaN) with two formula units in the primitive cell is described by the space group  $C_{6v}^4$ . At the center of the Brillouin zone the nine optical phonons belong to the following irreducible representation:<sup>50,51</sup>

$$\Gamma_{\text{opt}} = 1A_1 + 2B_1 + 1E_1 + 2E_2.$$

Both  $A_1$  and  $E_1$  modes are polar, that is, they are split into TO and LO modes with different frequencies due to the macroscopic electric fields associated with the longitudinal phonons. The short-range interatomic forces cause the mode anisotropy, that is, the  $A_1$  and  $E_1$  modes possess different frequencies. Because the electrostatic forces dominate the anisotropy in the short-range forces, the TO-LO splitting is larger than the  $A_1$ - $E_1$  splitting. For the lattice vibrations with  $A_1$  and  $E_1$  symmetry, the atoms move parallel and perpendicular to the  $\alpha$ -GaN  $c$  axis, respectively. Both  $A_1$  and  $E_1$  modes are Raman and ir-active. The two nonpolar ir-inactive  $E_2$  modes ( $E_2^{(1)}, E_2^{(2)}$ ) are Raman-active. Note that only the  $E_2^{(2)}$  mode is within the spectral range studied in this work. The  $B_1$  modes are ir- and Raman-inactive (silent modes).

### B. ir dielectric lattice response

The frequencies of the TO and LO modes correspond to poles and zeros of the material dielectric function  $\epsilon(\omega)$ , respectively.<sup>31,52</sup> The amount of the TO-LO frequency splitting is a measure of the polar strength of the phonon branches.<sup>4,31,53</sup> The contribution of  $l$  polar crystal lattice modes to the infrared dielectric response  $\epsilon^{(L)}$  at photon energy  $\hbar\omega$  can be described using a factorized model with Lorentzian broadening ( $j = \parallel, \perp$ ),<sup>45,46</sup>

$$\epsilon_j^{(L)}(\omega) = \epsilon_{\infty,j} \prod_{i=1}^l \frac{\omega^2 + i\gamma_{\text{LO},ij}\omega - \omega_{\text{LO},ij}^2}{\omega^2 + i\gamma_{\text{TO},ij}\omega - \omega_{\text{TO},ij}^2}, \quad (1)$$

where  $\omega_{\text{LO},ij}$ ,  $\gamma_{\text{LO},ij}$ ,  $\omega_{\text{TO},ij}$ , and  $\gamma_{\text{TO},ij}$  are the frequency and the broadening value of the  $i$ th LO and TO phonon,

respectively. In this work the parameters  $\omega_{\text{TO},\parallel}$ ,  $\omega_{\text{TO},\perp}$ ,  $\omega_{\text{LO},\parallel}$ , and  $\omega_{\text{LO},\perp}$  denote the frequencies of the  $\alpha$ -GaN  $A_1(\text{TO})$ ,  $E_1(\text{TO})$ ,  $A_1(\text{LO})$ , and  $E_1(\text{LO})$  modes, respectively, and the model parameters  $\epsilon_{\infty,\parallel}$  and  $\epsilon_{\infty,\perp}$  are the high-frequency limits for polarization parallel and perpendicular to the  $\alpha$ -GaN  $c$  axis, respectively. A slightly different but common description of the lattice contribution to the ir dielectric function is given by the sum of harmonic Lorentz oscillators,<sup>14,45,46</sup>

$$\epsilon_j(\omega) = \epsilon_{\infty,j} \sum_{i=1}^{\alpha} \frac{S_{ij}\omega_{\text{TO},ij}^2}{\omega_{\text{TO},ij}^2 - \omega^2 - i\omega\Gamma_{ij}}, \quad (2)$$

where  $S_{ij}$  denotes the strength,  $\omega_{\text{TO},ij}$  the TO-phonon frequency, and  $\Gamma_{ij}$  the damping constant of the  $i$ th lattice mode. Note that Eqs. (1) and (2) become identical if  $\Gamma_i = \gamma_{\text{TO},i} \approx \gamma_{\text{LO},i} \ll \omega_{\text{TO},i}$ . The expression for  $\epsilon$  in Eq. (1) descends from consideration of anharmonic coupling effects of TO and LO phonons in multiple-phonon-mode materials.<sup>46</sup> The sum of harmonic Lorentz oscillators in Eq. (2) can be transformed into a similar factorized form by partial fraction decomposition. The parameters  $\gamma_{\text{LO},ij}$ , however, are then tied to all other harmonic oscillator parameters and are not independent of each other. The harmonic approximation excludes the anharmonic effect of phonon coupling and fails to describe the typically asymmetric dielectric response function of multiple-mode materials especially near phonon-mode frequencies. (For a plausible discussion using a classical two-optical-mode oscillator model see Barker and Hopfield.<sup>44</sup>) In order to keep the physical meaning of  $\epsilon(\omega)$  in Eq. (1), i.e., to yield  $\text{Im}\{\epsilon^{(L)}(\omega)\}|_{\omega \rightarrow \infty} \geq 0$ , the generalized Lowndes condition needs to be satisfied:<sup>43,54</sup>

$$\sum_{i=1}^l \gamma_{\text{LO},i} \geq \sum_{i=1}^l \gamma_{\text{TO},i}. \quad (3)$$

If we require that  $\epsilon$  does not contain terms proportional to  $1/\omega$  for  $|\omega| \rightarrow \infty$ , the inequality sign in the above expression is no longer valid and has to be replaced by the equal sign.<sup>49</sup>

### C. Free-carrier contribution

The contribution of one free-carrier species to the dielectric function  $\epsilon^{(\text{FC})}$  is commonly written in the classical Drude approximation<sup>31,52</sup>

$$\epsilon_j^{\text{FC}}(\omega) = -\epsilon_{\infty,j} \frac{\omega_{p,j}^2}{\omega(\omega + i\gamma_{p,j})}, \quad (4)$$

with

$$\omega_{p,j} = \left( \frac{Ne^2}{\epsilon_{\infty,j}\epsilon_0 m_j} \right)^{1/2}. \quad (5)$$

The screened plasma frequencies  $\omega_{p,j}$  depend on the free-carrier concentration  $N$ ,  $\epsilon_{\infty,j}$ , and the effective mass  $m_j$  of the free carriers ( $\epsilon_0$  is the vacuum permittivity and  $e$  the electrical unity charge). The plasmon broadening parameters  $\gamma_{p,j}$  are related to the inverse of the energy-averaged carrier-momentum relaxation time  $\langle \tau_m \rangle_j$ . We assume a constant-carrier-scattering regime, and substitute  $\langle \tau_m \rangle_j$  by the optical carrier mobility  $\mu_j$ :<sup>4,53</sup>

$$\gamma_{p,j} \equiv (\langle \tau_m \rangle_j)^{-1} = \frac{e}{m_j \mu_j}. \quad (6)$$

Plasmons strongly interact with LO phonons when  $\omega_p$  is in the range of the lattice TO and LO modes. LO-phonon-plasmon (LPP) coupling has been observed in  $n$ -type  $\alpha$ -GaN by several authors using Raman spectroscopy.<sup>16–19</sup> However, the LPP modes can only be observed in Raman spectra when the plasmon is not too greatly damped. Especially in the case of  $p$  doping, overdamping of plasmons ( $\omega_p \ll \gamma_p$ ) occurs because of small free-hole densities due to high acceptor activation energies and usually lower-mobility values of holes compared to electrons.<sup>22–24</sup> Kukharskii<sup>47</sup> suggested that the dielectric function for semiconductors with free carriers can be transformed into a factorized expression similar to that described above to allow for anharmonic coupling effects of plasmon excitations with LO phonons in multiple-polar-phonon-mode materials ( $k$  species of free carriers,  $l$  lattice phonon bands):

$$\begin{aligned} \epsilon_j^{(L+FC)}(\omega) &= \epsilon_{\infty,j} \frac{\prod_{i=1}^{k+l} (\omega^2 + i\tilde{\gamma}_{LO,ij}\omega - \tilde{\omega}_{LO,ij}^2)}{\omega^k \prod_{s=1}^k (\omega + i\gamma_{p,sj}) \prod_{i=1}^l (\omega^2 + i\gamma_{TO,ij}\omega - \omega_{TO,ij}^2)}, \end{aligned} \quad (7)$$

where  $\tilde{\omega}_{LO,ij}$  and  $\tilde{\gamma}_{LO,ij}$  are the eigenfrequencies and the broadening values of the  $(k+l)$  LPP modes, respectively. The  $\gamma_{p,sj}$  values are treated as the plasmon broadening parameters in the long-wavelength limit. Kukharskii successfully applied Eq. (7), and observed the anharmonic character of LPP modes within reflection data of low to moderately and heavily doped GaAs.<sup>47</sup> For  $n$ - and  $p$ -type  $\alpha$ -GaN ( $k=l=1$ ), the LPP-mode frequencies  $\tilde{\omega}_{LO,ij}$  in Eq. (7) are the well-known roots of  $\epsilon_j = \epsilon_j^{(L)} + \epsilon_j^{(FC)}$ , if damping is neglected ( $\gamma_{TO,j} = \gamma_{LO,j} = \gamma_{p,j} = 0$ ;  $i=1,2$ ;  $j=\perp, \parallel$ ):

$$\begin{aligned} \tilde{\omega}_{LO,ij} &= \{0.5[\omega_{LO,j}^2 + \omega_{p,j}^2 \\ &+ (-1)^i \sqrt{(\omega_{LO,j}^2 + \omega_{p,j}^2)^2 - 4\omega_{p,j}^2 \omega_{TO,j}^2}]\}^{0.5}, \end{aligned} \quad (8)$$

where  $\tilde{\omega}_{LO,1j}$  ( $\tilde{\omega}_{LO,2j}$ ) is the screened frequency of the lower (upper) LPP mode branch. Equations (5)–(8) connect  $N$ ,  $m_j$ , and  $\mu_j$  with  $\epsilon_j^{L+FC}(\omega)$ . Note that only the quantities  $N/m_j$  and  $N\mu_j$  can be determined from the plasma frequency and broadening parameter independently. The effective mass and mobility parameters can only be obtained when the carrier concentration  $N$  is known. Likewise,  $N$  can be determined when the effective mass and/or mobility values are known. Note further that  $\epsilon_{\infty,j}$  can affect the free-carrier parameter results when an incorrect value is assumed.

#### D. Impurity modes

Equation (8) is no longer valid for materials with more than one ir-active phonon band ( $l > 1$ ). ir-active modes ( $\nu = 1, \dots, n$ ) with small LO-TO splitting values  $\delta\omega_\nu^2 = \omega_{LO,\nu}^2 - \omega_{TO,\nu}^2$ , i.e., modes with low polarity such as impurity

modes (IM,  $\omega_{IM,\nu} \equiv \omega_{TO,\nu}$ ), contribute to the dielectric function as a small perturbation only

$$\begin{aligned} \epsilon_j^{(L+FC+IM)}(\omega) &= \epsilon_j^{(L+FC)}(\omega) \prod_{\nu=1}^n \\ &\times \left( 1 + \frac{i\delta\gamma_{\nu,j}\omega - \delta\omega_{\nu,j}^2}{\omega^2 + i\gamma_{IM,\nu j}\omega - \omega_{IM,\nu j}^2} \right), \end{aligned} \quad (9)$$

where we introduced a broadening parameter  $\delta\gamma_\nu \equiv \gamma_{LO,\nu} - \gamma_{TO,\nu}$ . For  $\delta\gamma_\nu \sim 0$ , and small  $\text{Im}\{\epsilon_j^{(L+FC)}\}$  values for  $\omega \sim \omega_{IM,\nu}$ , it follows from Eq. (8) that  $\delta\omega_\nu^2 < 0$  ( $\delta\omega_\nu^2 > 0$ ) if the frequency of the IM is within the spectral range  $\omega_{TO,i} < \omega_{IM,\nu} < \omega_{LO,i}$  ( $\omega_{LO,i} < \omega_{IM,\nu} < \omega_{TO,i+1}$ ). If contributions due to IM's are present within experimental spectra, but neglected during data analysis, then it can be read from Eq. (9) that a new ‘‘high-frequency’’ limit value  $\tilde{\epsilon}_{\infty,j}$  will result from the line-shape fit

$$\tilde{\epsilon}_{\infty,j}(\omega=0) = \epsilon_{\infty,j} \prod_{\nu=1}^n \left( 1 + \frac{\delta\omega_{\nu,j}^2}{\omega_{IM,\nu j}^2} \right). \quad (10)$$

Accordingly,  $\tilde{\epsilon}_{\infty,j}$  will be too small (too large) for IM's not considered but located within  $\omega_{TO,i} < \omega_{IM,\nu} < \omega_{LO,i}$  ( $\omega_{LO,i} < \omega_{IM,\nu} < \omega_{TO,i+1}$ ). Appropriate consideration of low polar IM's allows us to derive the screened plasma frequencies  $\omega_{p,j}$ , and one obtains for the  $l=1$  lattice phonon band and  $n$  impurity modes

$$\omega_{p,j} = \sqrt{\frac{Ne^2}{\epsilon_{\infty,j}\epsilon_0 m_j} \prod_{\nu=1}^n \left( 1 + \frac{\delta\omega_{\nu,j}^2}{\omega_{IM,\nu j}^2} \right)^{0.5}}. \quad (11)$$

From the requirement  $\text{Im}\{\epsilon_j^{(L+FC+IM)}\}|_{\omega \rightarrow \infty} \geq 0$ , one can derive the following constraint for  $\delta\gamma_\nu$ , regardless of  $\delta\omega_\nu^2$ ,

$$\sum_{i=1}^{k+l} (\tilde{\gamma}_{LO,ij} - \gamma_{TO,ij}) + \sum_{\nu=1}^n \delta\gamma_{\nu j} \geq 0. \quad (12)$$

#### E. SE data analysis

Ellipsometry determines the complex ratio  $\rho$  of the reflection coefficients for light polarized parallel ( $R_p$ ) and perpendicular ( $R_s$ ) to the plane of incidence.<sup>42</sup> The result of an ellipsometry measurement is usually presented by the ellipsometric parameters  $\Psi$  and  $\Delta$ , where  $\tan \Psi$  is defined as the absolute value of  $\rho$ , and  $\Delta$  denotes the relative phase change of the  $p$  and  $s$  components of the electric field vector upon reflection:<sup>42</sup>

$$\rho = \frac{R_p}{R_s} = \tan \Psi \exp(i\Delta). \quad (13)$$

In addition to  $\Psi$  and  $\Delta$ , their standard deviations  $\sigma_i^\Psi$  and  $\sigma_i^\Delta$  are measured.<sup>38,40</sup> The parameters  $\Psi$  and  $\Delta$  depend on the photon energy  $\hbar\omega$ , the layer sequence within the sample, the dielectric function  $\epsilon$  and thickness  $d$  of each layer, the dielectric function of the substrate material that supports the layer stack, and the angle of incidence  $\Phi$ .

In principle, the thickness and dielectric function of each sample layer can be determined from an ellipsometry experiment by comparing calculated data to measured data. Tradi-

tionally, point-by-point fits are performed where the dielectric function values of interest are extracted from the experimental data for each wavelength and independent of all other spectra data points. For this procedure, the thicknesses and dielectric functions of all other sample constituents have to be known. The dielectric function obtained from the point-by-point fit then needs further comparison with model assumptions in order to obtain values of physically relevant parameters such as phonon-mode frequencies and broadening parameters. However, fitting parametrized model dielectric functions to experimental data, simultaneously for all spectral data points, provides direct connection between measured data and physical parameters of interest. Parametric models further prevent wavelength-by-wavelength measurement noise from becoming part of the extracted dielectric functions. Parametric model assumptions greatly reduce the number of free parameters. However, the use of parametric models involves a certain risk for subtle spectral features to be subsumed by the line shape of the model function. Nevertheless, parametrization of  $\epsilon$  based on a physical model is the best choice for SE data analysis, especially when the point-by-point fit method is inapplicable. The standard model for analyzing SE data is based on a sequence of homogeneous layers with smooth and parallel interfaces. For anisotropic materials, the ellipsometric measurements depend on the principal-axis dielectric functions  $\epsilon_x$ ,  $\epsilon_y$ , and  $\epsilon_z$ , the orientation of the crystal principal axes with respect to the plane of incidence, and the polarization state of the incident light beam.<sup>39,42,55</sup> For a general situation of optical anisotropy and sample orientation the simple definition of  $\rho$  in Eq. (13) is no longer a complete description, and a generalized ellipsometry approach is needed.<sup>39,42,55,56</sup> Due to the uniaxial symmetry of hexagonal GaN, two of its principal dielectric functions, the extraordinary  $\epsilon_{\parallel}$  (parallel to the  $c$  axis) and the ordinary  $\epsilon_{\perp}$  (perpendicular to the  $c$  axis), differ from each other. Here, point-by-point fits are inapplicable because the number of available independent parameters ( $\Psi$  and  $\Delta$  for every wavelength regardless of the angle of incidence) is less than the amount of information wanted (the complex GaN dielectric functions  $\epsilon_{\parallel}$  and  $\epsilon_{\perp}$  and the layer thickness  $d$ ). The only solution is the use of parametric model assumptions. Two sets of model phonon parameters (frequencies and broadening values of the  $E_1$  and  $A_1$  modes), free-carrier parameters ( $m_j, \mu_j$ ), and two high-frequency values  $\epsilon_{\infty, j}$  are required. It has to be noted that not all of the model parameters for  $\epsilon_{\parallel}$  and  $\epsilon_{\perp}$  can be obtained from our ellipsometry data due to the crystal axes orientation of the uniaxial GaN films studied here.

Because of the high-symmetry orientation of the birefringent  $c$ -plane sapphire substrate, both crystal principal-axis coordinate systems of sapphire and  $\alpha$ -GaN coincide with the ellipsometry laboratory coordinate system. Both  $c$  axes and the sample normal are collinear, and a single complex ratio as in Eq. (13) is sufficient. The Levenberg-Marquardt algorithm<sup>57</sup> is used to fit the model parameters for  $\epsilon_{\parallel}$  and  $\epsilon_{\perp}$  of  $\alpha$ -GaN by minimizing the following weighted test function (maximum likelihood approach):

$$\xi^2 = \frac{1}{2S - K} \sum_{i=1}^S \left[ \left( \frac{\Psi_i - \Psi_i^c}{\sigma_i^{\Psi}} \right)^2 + \left( \frac{\Delta_i - \Delta_i^c}{\sigma_i^{\Delta}} \right)^2 \right]. \quad (14)$$

$S$  denotes the number of measured  $(\Psi_i, \Delta_i)$  data pairs,  $K$  is the number of real-valued fit parameters, and  $\Psi_i^c$  and  $\Delta_i^c$  are the calculated ellipsometric parameters at photon energy  $\hbar\omega_i$ .<sup>40,41</sup> Issues of parameter accessibility from spectroscopic ellipsometry data have been thoroughly discussed by Jellison (see Ref. 38 and references therein; see also Ref. 58.) The random experimental errors  $(\sigma_i^{\Psi}, \sigma_i^{\Delta})$  were propagated into the error bars on our fit parameters. These error bars also represent finite correlation values between the fit parameters. The light propagation within the sample is calculated using a standard matrix formalism for anisotropic multilayered systems with plane-parallel interfaces.<sup>38,39</sup> The sapphire dielectric functions, which are prerequisites for the model calculations, were determined previously by IRSE.<sup>43</sup>

### III. EXPERIMENT

Four  $\alpha$ -GaN films (samples A–D) were grown on (0001) $\alpha$ -Al<sub>2</sub>O<sub>3</sub> substrates without buffer layers by plasma-assisted molecular beam epitaxy (MBE). The thickness of the  $\alpha$ -GaN films varies between 0.8 and 1.5  $\mu\text{m}$ . An approximately 1- $\mu\text{m}$ -thick titanium layer was deposited at the unpolished backside of the sapphire substrate. This layer does not affect the IRSE spectra in the spectral range studied here and is not considered during our model calculations. Samples A and B were nominally undoped, whereas a high concentration of Mg was used to obtain a  $p$ -type conductive film (sample C,  $N_h \sim 8 \times 10^{17} \text{ cm}^{-3}$ ). Sample D was Si doped and highly  $n$ -type conductive ( $N_e \sim 1 \times 10^{19} \text{ cm}^{-3}$ ). Hall measurements were performed on all samples, and the free-carrier concentrations obtained there are given in Table I.

The IRSE spectra were recorded at room temperature in the wave-number range between 300 and 1200  $\text{cm}^{-1}$  with a spectral resolution of 2  $\text{cm}^{-1}$ , and at 72° angle of incidence. A rotating-polarizer, rotating-compensator type, Fourier-transform spectroscopic ellipsometer was utilized (J. A. Woollam Co.<sup>59</sup>). Micro-Raman measurements were performed at room temperature on each sample. The spectra were recorded in the  $z(x, x)\bar{z}$  backscattering configuration,<sup>50</sup> where the  $z$  direction was oriented along the hexagonal  $c$  axis of the GaN film. The 458-nm line of an Ar laser was used for excitation, and the incident laser power was about 100 mW. The beam was focused onto the sample surface, and the probe-beam spot size was about 1.5  $\mu\text{m}$ . The scattered light was recorded with an XY Dilor spectrometer. The micro-Raman spectra were analyzed with Lorentzian line shapes to estimate the center frequencies of the Raman peaks.

### IV. RESULTS AND DISCUSSION

Figures 1 and 2 show experimental and calculated  $\Psi$  and  $\Delta$  spectra of all samples in the frequency range from 300 to 1200  $\text{cm}^{-1}$ , which is strongly affected by lattice and free-carrier excitations. Note the excellent agreement between measured and calculated data. IRSE spectra of  $\alpha$ -Al<sub>2</sub>O<sub>3</sub>( $S$ ) are included for comparison. Brackets mark the ir-active sapphire phonon modes of  $A_{2u}$  and  $E_u$  symmetry. The experimental spectra were recorded as described in Sec. III, and the calculated data were obtained using a two-phase model (ambient/substrate) for  $c$ -plane sapphire ( $S$ ), and a three-phase model (ambient/film/substrate) for samples A–C. The

TABLE I. Hall results and best-fit values from the IRSE data regression analysis for the free-carrier parameters and the high-frequency dielectric constants. The error limits, which correspond to 90% reliability, are given in parentheses.

Sample	Type	$N(300\text{ K})$ ( $10^{17}\text{ cm}^{-3}$ )		$\mu_{\perp}$	$\mu_{\parallel}$	$m_{\perp}$	$m_{\parallel}$	$\epsilon_{\infty,\perp}$	$\epsilon_{\infty,\parallel}$
		IRSE	Hall						
A	$n^a$	0.78 (0.06)	b	$71^c$ (15)	$71^c$ (15)	$0.22^d$	$0.22^d$	5.04 (0.02)	5.01 (0.04)
B	$n$	3.2 (0.7)	2	$58^c$ (12)	$58^c$ (12)	$0.22^d$	$0.22^d$	4.94 (0.05)	4.92 (0.011)
C	$p$	$8^d$	8	$10^c$ (3)	$10^c$ (3)	$1.40^c$ (0.33)	$1.40^c$ (0.33)	5.22 (0.03)	5.37 (0.06)
D	$n$	$100^d$	100	127 (6)	122 (13)	0.237 (0.006)	0.228 (0.008)	5.20 (0.11)	5.18 (0.21)

<sup>a</sup>Free carriers are assumed to be electrons.

<sup>b</sup>Not detectable.

<sup>c</sup>Isotropically averaged, IRSE data have no sensitivity to free-carrier parameter anisotropy.

<sup>d</sup>Assumed values, not varied during data analysis.

anisotropic  $\alpha$ -GaN dielectric functions were factorized through Eq. (7). For sample *D*, a four-phase model (ambient/depletion layer/film/substrate) was employed. Here, a carrier-depleted thin  $\alpha$ -GaN surface layer was considered, for which the dielectric function was calculated by Eq. (1). Three additional ir-active phonon modes were observed within the highly-Si-doped  $\alpha$ -GaN layer of sample *D*, and the dielectric

function was modeled by Eq. (9), i.e., IM's with low polarity are included here. Figure 3 enlarges the impurity-mode region of sample *D*. If additional modes are neglected during analysis of sample *D*, i.e., if Eq. (7) instead of Eq. (9) is used, the resulting fit is poor, as shown in Fig. 3(a). Further details of our sample analysis follow below. Figure 4 shows the micro-Raman spectra of all samples and of *c*-plane  $\alpha$ -Al<sub>2</sub>O<sub>3</sub>(*S*) for comparison. The  $\text{Im}\{\epsilon_{\perp}\}$  and  $\text{Im}\{-1/\epsilon_{\perp}\}$  spectra of all four  $\alpha$ -GaN layers, which were obtained from

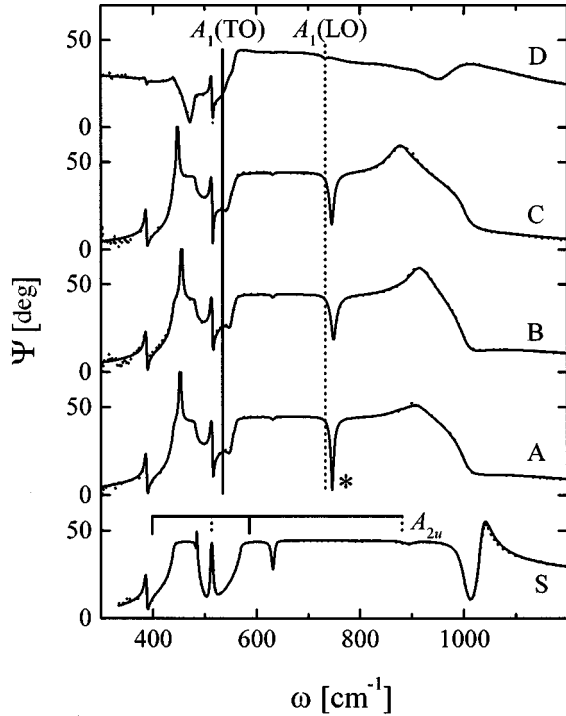


FIG. 1. Experimental (dotted lines) and calculated (solid lines) IRSE  $\Psi$  spectra of all samples at a  $72^\circ$  angle of incidence (A,  $N_e = 7.8 \times 10^{16}\text{ cm}^{-3}$ ; B,  $N_e = 3.2 \times 10^{17}\text{ cm}^{-3}$ ; C,  $N_h = 8 \times 10^{17}\text{ cm}^{-3}$ ; D,  $N_e = 1 \times 10^{19}\text{ cm}^{-3}$ ). The spectra of *c*-plane sapphire are included for comparison (*S*). The transverse and longitudinal  $A_{2u}$  phonon modes of sapphire are indicated by brackets (solid brackets, TO; dotted brackets, LO). The dip marked by an asterisk arises from the  $\alpha$ -GaN high-frequency  $A_1$ -LPP mode.

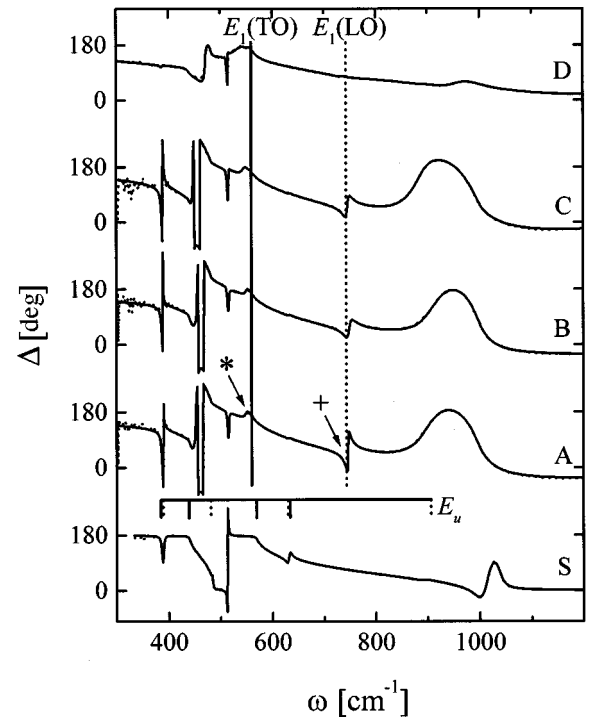


FIG. 2. Same as Fig. 1 for  $\Delta$ . The spectra of *c*-plane sapphire are included for comparison (*S*). The transverse and longitudinal  $E_u$  phonons of sapphire are indicated by brackets (solid brackets, TO; dotted brackets, LO). The small peak marked by an asterisk is due to the  $\alpha$ -GaN  $E_1$ (TO) mode; the structure marked by a cross stems from the  $\alpha$ -GaN high-frequency  $A_1$ -LPP mode.

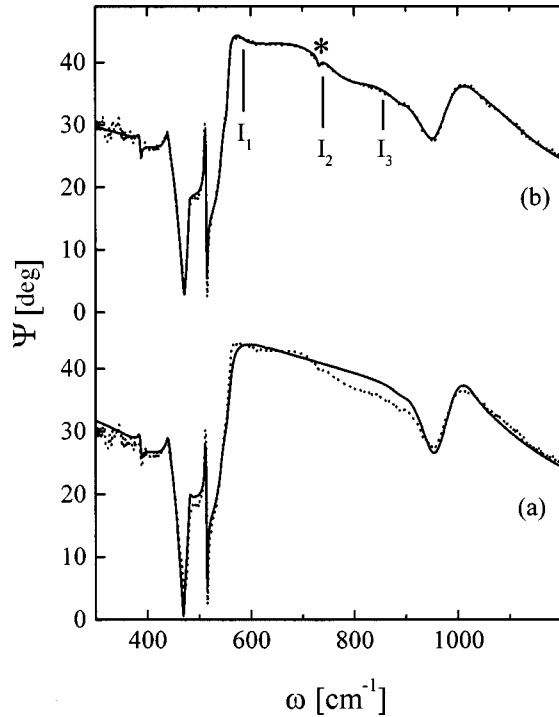


FIG. 3. Experimental (dotted lines) and calculated (solid lines) IRSE  $\Psi$  spectra of sample  $D$  ( $N_e = 1 \times 10^{19} \text{ cm}^{-3}$ ) at a  $72^\circ$  angle of incidence. (a) The anharmonic model [Eq. (7)] with one free-carrier species ( $k=1$ ) and one lattice LO phonon ( $l=1$ ) was used for the calculation, which leads only to a poor fit. (b) Three additional ir-active modes ( $I_1, I_2, I_3$ ) were included in the calculation, which considerably improved the line-shape fit. The small dip (marked by an asterisk) stems from the unscreened  $A_1(\text{LO})$  mode, which is assigned to a thin  $\alpha$ -GaN surface depletion layer.

the data analysis using the factorized model, are depicted in Fig. 5. Figure 6 compares the results of the model calculation for samples  $A$  and  $D$  between the parametrization of the  $\alpha$ -GaN dielectric function using the anharmonic model based on Eq. (1) and the harmonic model based on Eq. (2). In the case of the low-conductivity films, such as for sample  $A$ , both approximations provide good line-shape fits because of  $\gamma_{\text{TO}} \approx \tilde{\gamma}_{\text{LO},2}$  and  $\gamma_p \approx \tilde{\gamma}_{\text{LO},1}$  (see Table III). However, for the high-conductivity  $\alpha$ -GaN film (sample  $D$ ) no appropriate description of the experimental data can be achieved using the harmonic model approach, especially in the spectral range where the three additional modes occur.

The model parameters that were allowed to vary during data analysis are the  $E_1(\text{TO})$ ,  $A_1(\text{LO})$ , and  $E_1(\text{LO})$  phonon frequencies, the anisotropic broadening values of the LPP modes, the  $E_1(\text{TO})$  mode, and plasmon-broadening parameters. The LPP mode frequencies were then calculated using Eq. (8) and the plasma frequencies using Eq. (5). The  $A_1(\text{TO})$  phonon-mode resonance could not be found due to the geometry of the experiment (see below). Similar to the Barker and Ilegems work, the  $A_1(\text{TO})$  frequency was taken from Raman results.<sup>14</sup> For the nominally undoped, but low-conductivity  $n$ -type samples  $A$  and  $B$  we fitted  $N_e$  and  $\mu_j$  assuming  $m_e/m_0 = 0.22$ . For samples  $C$  and  $D$  we assumed the  $N$  values obtained from our Hall measurements and fitted  $\mu_j$  and  $m_j$ . The  $\alpha$ -GaN layer thicknesses were also allowed to vary. Despite the apparently large number of unknown

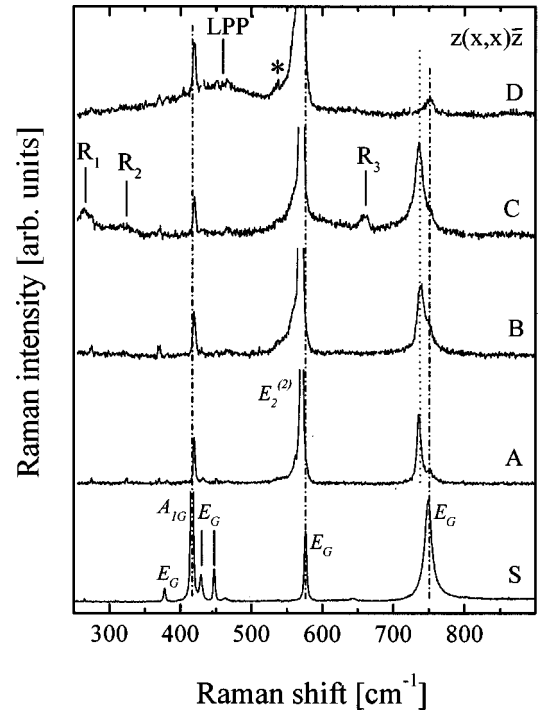


FIG. 4. Room-temperature micro-Raman spectra of unintentionally doped ( $A, B$ ),  $p$ -type ( $C$ ), and  $n$ -type ( $D$ )  $\alpha$ -GaN. The Raman spectrum of  $c$ -plane sapphire is included for comparison ( $S$ ). Dashed-dotted lines mark the strongest sapphire-related Raman peaks. While the  $A_1(\text{LO})$  mode (dotted line) disappears, the lower  $A_1$ -LPP mode (LPP $^-$ ) occurs at  $459 \text{ cm}^{-1}$  within the spectrum of  $n$ -type sample  $D$  ( $N_e = 1 \times 10^{19} \text{ cm}^{-3}$ ). The asterisk marks the forbidden  $A_1(\text{TO})$  mode (spectrum  $D$ ).

parameters, we obtained very stable fits, because the number of independent data points acquired during the ellipsometry measurement exceeds by far the number of fit parameters. Note also that in contrast to ir-reflectometry experiments, ellipsometry does not have to rely on the intensity of the light source.<sup>32,60</sup> The best-fit parameter values, and those that follow accordingly (such as the LPP mode and plasma frequencies) for the samples  $A$ – $D$  are given in Table I–IV. The sapphire dielectric functions were taken from Ref. 43.

Due to the crystal-axis orientation of the GaN films not all of the model parameters can be obtained here. In particular, the ellipsometry data from the  $c$ -plane-oriented films have no sensitivity to the TO resonance frequency with polarization vector parallel to the sample normal. Except for wavelengths where the real part of  $\epsilon_{\parallel}$  is between 0 and 1 for wave numbers above the LO-phonon frequency, the incident light beam propagates almost parallel to the sample normal within the film and senses mostly  $\epsilon_{\perp}$ . The lattice displacement pattern that belongs to the TO resonance in  $\epsilon_{\parallel}$  cannot be excited by the ir light beam in this configuration. In contrast, the LO-mode frequency in  $\epsilon_{\parallel}$  can be located precisely through the well-known Berreman effect in thin polar dielectric films.<sup>61</sup> The incident wave is guided along the thin-film interfaces near wave numbers where the index of refraction of the extraordinary direction approaches unity. This effect causes distinct features within the  $p$ -polarized reflectivity. In this spectral region the ellipsometry data provide high sensitivity to the LO-phonon frequency and broadening parameters for  $\epsilon_{\parallel}$ . The LO-mode parameters for  $\epsilon_{\perp}$  follow from

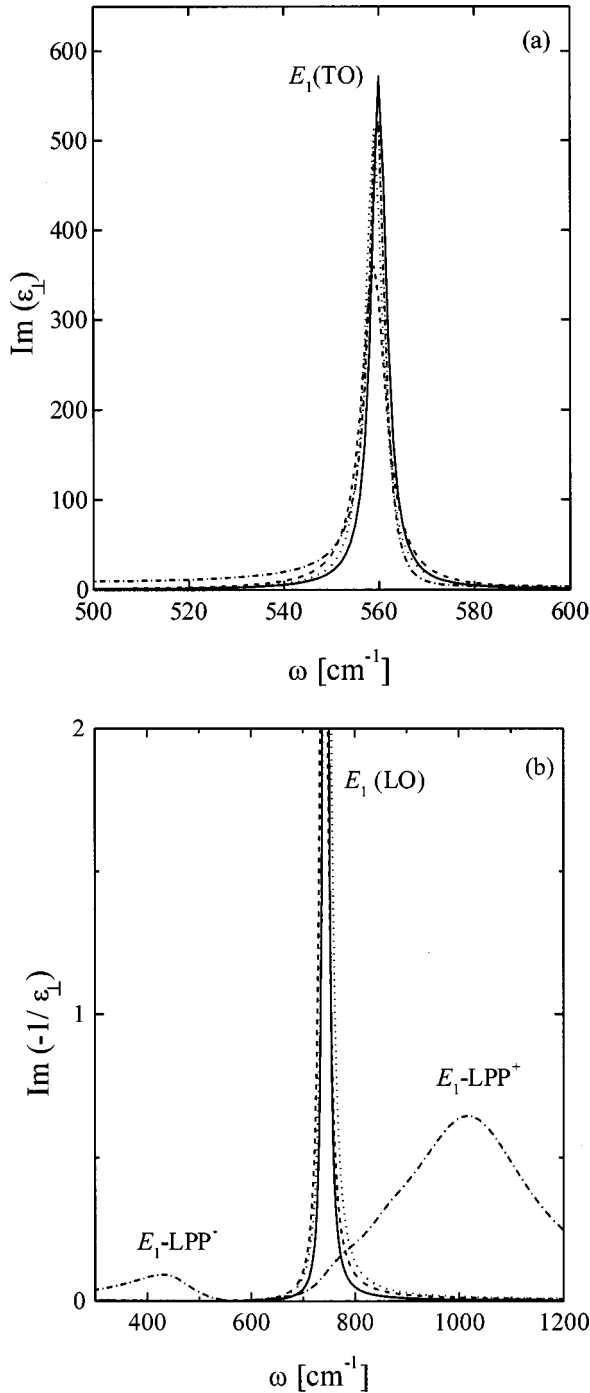


FIG. 5. (a)  $\text{Im}\{\epsilon_{\perp}\}$  and (b)  $\text{Im}\{-1/\epsilon_{\perp}\}$  spectra of all  $\alpha$ -GaN layers obtained from the best-fit data analysis using the anharmonic model [Eq. (7) for samples A–C, and Eq. (9) for sample D]. Sample A, solid lines; B, dotted lines; C, dashed lines; D, dash-dotted lines.

the “strength” of the TO mode, which is in resonance during the ir experiment. Thus, the frequency and broadening parameter of the  $A_1(\text{TO})$  mode for  $c$ -plane-oriented films are needed as input parameters for analysis of the ir dependence of  $\epsilon_{\parallel}$ .

The IRSE spectra of the  $\alpha$ -GaN films on  $\alpha$ - $\text{Al}_2\text{O}_3$  provide high sensitivity to the frequencies and broadening values of the ir-active  $E_1(\text{TO})$  mode and coupled  $A_1$ -LPP( $\tilde{\omega}_{\text{LO},i\parallel}$ ) and  $E_1$ -LPP( $\tilde{\omega}_{\text{LO},i\perp}$ ) modes. (Vertical lines in Figs. 1 and 2 in-

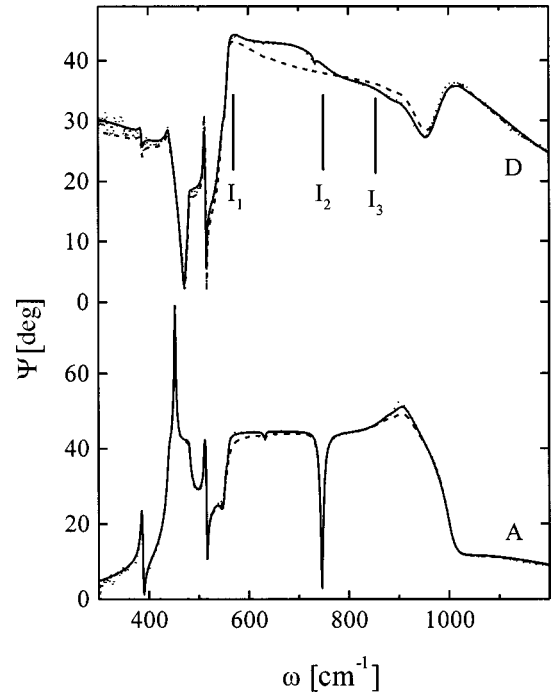


FIG. 6. IRSE  $\Psi$  spectra of the low-conductivity sample A ( $N_e = 7.8 \times 10^{16} \text{ cm}^{-3}$ ) and high-conductivity sample D ( $N_e = 1 \times 10^{19} \text{ cm}^{-3}$ ) at a  $72^\circ$  angle of incidence. For sample A both the anharmonic model (solid lines) and the harmonic model (dashed lines) lead to good line-shape fits, whereas for sample D only the use of the anharmonic model approach including contributions of additional modes [Eq. (9)] is appropriate. Experimental data are shown by dotted lines.

dicating the spectral positions of the uncoupled ir-active  $\alpha$ -GaN modes and are included to guide the eye.) Samples A and B reveal only a small concentration of free carriers. Here, the high-frequency LPP modes  $\tilde{\omega}_{\text{LO},2\perp}$  and  $\tilde{\omega}_{\text{LO},2\parallel}$  are virtually identical with  $E_1(\text{LO})$  and  $A_1(\text{LO})$ , respectively. For high-resistivity  $\alpha$ -GaN resonant excitation of the  $E_1(\text{TO})$  and  $A_1(\text{LO})$  phonons by the IRSE probe beam causes resonancelike features within the  $\Psi$  and  $\Delta$  spectra. For example, the features in  $\Psi$  [ $\Delta$ ] marked by asterisks in Fig. 1 [Fig. 2] stem from the  $A_1(\text{LO})$  [ $E_1(\text{TO})$ ] mode, but no spectral structure can be directly attributed to the  $E_1(\text{LO})$  and  $A_1(\text{TO})$  mode. Although apparently located close to the  $E_1(\text{LO})$  frequency, the feature in  $\Delta$  of sample A marked by a cross is due to the  $A_1(\text{LO})$  mode resonance (Fig. 2). As discussed in detail by Barker and Ilegems,<sup>14</sup> the  $E_1(\text{LO})$  mode parameters can still be obtained from line-shape analysis of the sample dielectric response over the high-frequency edge of the reststrahlen spectral range. The  $A_1(\text{TO})$  mode frequency and broadening values cannot be obtained from the IRSE spectra. We therefore assumed  $\omega_{\text{TO},\parallel} = 537 \text{ cm}^{-1}$  from our Raman measurements. No information is available for the broadening value, and we assumed  $\gamma_{\text{TO},\parallel} = 4 \text{ cm}^{-1}$ , which is a typical  $\gamma_{\text{TO},\perp}$  value observed here.

The micro-Raman spectra of samples A–C in Fig. 4 in the  $z(x,x)\bar{z}$  backscattering geometry exhibit the allowed high-frequency  $A_1$ -LPP mode ( $\tilde{\omega}_{\text{LO},2\parallel}$ ; dotted line) and the  $E_2^{(2)}$  mode. Due to the large aperture of the incident micro-Raman beam, symmetry-forbidden modes such as the  $E_1(\text{TO})$  mode (the shoulder at the low-frequency side of the

TABLE II. Best-fit values from the IRSE data regression analysis for the layer thickness  $d$  and the  $\alpha$ -GaN lattice phonon frequencies. The error limits, which correspond to 90% reliability, are given in parentheses.

Sample	$d$ (nm)		$\omega_{\text{TO},\perp}$	$\omega_{\text{LO},\perp}$	$\omega_{\text{TO},\perp}$	$\omega_{\text{LO},\parallel}$
	IRSE	Nominal	$[E_1(\text{TO})]$ ( $\text{cm}^{-1}$ )	$[E_1(\text{LO})]$ ( $\text{cm}^{-1}$ )	$[A_1(\text{TO})]$ ( $\text{cm}^{-1}$ )	$[A_1(\text{LO})]$ ( $\text{cm}^{-1}$ )
A	890(2)	960	560.1(0.2) 560.8 <sup>b</sup> (0.4)	742.1(0.3)	537 <sup>a</sup>	732.5(0.2)
B	827(6)	1000	559.0(0.4) 557.7 <sup>b</sup> (0.7)	738.4(1.5)	537 <sup>a</sup>	729.1(1.8)
C	997(3)	1000	558.9(0.2)	737.5(0.6)	537 <sup>a</sup>	730.6(0.8)
D	1414 <sup>c</sup> (24)	1440	559.8(0.3)	739 <sup>a</sup>	537 <sup>a</sup> 537.3 <sup>b</sup> (2.7)	732.0(1.6)

<sup>a</sup>Assumed value, not varied during data analysis.

<sup>b</sup>Obtained from Raman data.

<sup>c</sup>This value includes the carrier-depleted surface layer.

much stronger  $E_2^{(2)}$  mode) and the  $A_1(\text{TO})$  mode (marked by an asterisk in spectrum  $D$  at about  $537 \text{ cm}^{-1}$ ) occur. Although the laser beam was focused onto the top of the  $\alpha$ -GaN film, all Raman spectra are superimposed by sapphire modes (dash-dotted lines in Fig. 4). The IRSE spectra of our samples are highly influenced by the sapphire substrate too, but the GaN dielectric response can be separated from that of sapphire during data analysis using model assumptions as described above.

The IRSE spectra of the unintentionally doped  $\alpha$ -GaN samples  $A$  and  $B$  (Figs. 1 and 2) reveal very small free-carrier effects. Hence, the low-frequency LPP modes ( $\tilde{\omega}_{\text{LO},1j}$ ) as well as the screened plasma frequencies  $\omega_{pj}$  are very small, and the high-frequency LPP modes ( $\tilde{\omega}_{\text{LO},2j}$ ) differ from the lattice LO modes only by a few wave numbers. The IRSE best-fit values for the  $E_1(\text{TO})$  mode frequency (samples  $A$  and  $B$ ) and the values for the LPP-mode frequency  $\tilde{\omega}_{\text{LO},2\parallel}$  (samples  $A$  and  $B$ ) are in very good agreement with those observable within the micro-Raman spectra (Tables II and IV). The IRSE broadening values for the  $E_1(\text{TO})$  model ( $\gamma_{\text{TO},\perp}$ ) and the LPP modes ( $\tilde{\gamma}_{\text{LO},2\perp}$  and  $\tilde{\gamma}_{\text{LO},2\parallel}$ ) of sample  $A$  are smaller compared to those of sample  $B$ , indicating a better crystal quality of sample  $A$ . Accordingly, the linewidth of the Raman signals of sample  $A$  are smaller than those of sample  $B$ . For sample  $A$  the IRSE data analysis provided a small free-electron concentration value of  $N_e = (7.8 \pm 0.6) \times 10^{16} \text{ cm}^{-3}$ . The latter demonstrates that this optical technique possesses high sensitivity to free-carrier properties

even at low free-carrier concentration. The actual detection limits for the determination of free-carrier parameters depend on the effective carrier mass  $m$ , the carrier mobility  $\mu$ , and the layer thickness  $d$ . The value  $N_e = (3.2 \pm 0.7) \times 10^{17} \text{ cm}^{-3}$  determined by IRSE for sample  $B$  is in very good agreement with that obtained from Hall measurement ( $N_e = 2 \times 10^{17} \text{ cm}^{-3}$ ). The slightly larger ‘‘optical’’ value could be explained by an energy-dependent effective-electron-mass value that may be smaller than  $0.22m_0$  for small  $N_e$  values (a smaller assumed  $m_e$  value would decrease the best-fit parameter value  $N_e$ ; see also Sec. II C). Further IRSE experiments on differently Si-doped  $n$ -type  $\alpha$ -GaN films grown by metal-organic chemical vapor deposition (MOCVD) indicate such a dependence of  $m_e$  on  $N_e$ .<sup>62</sup>

The IRSE spectra of the  $p$ -type  $\alpha$ -GaN film (sample  $C$ ) are shown in Figs. 1 and 2. Following the same approach as used by Barker and Ilegems<sup>14</sup> and Perlin *et al.*<sup>15</sup> for  $n$ -type  $\alpha$ -GaN, we assumed here the Hall concentration value ( $N_h = 8 \times 10^{17} \text{ cm}^{-3}$ ) for our data analysis and fitted the hole mobility and the effective-hole-mass parameters. In the course of the data analysis we found only little information about the anisotropy of  $\mu$  and  $m_h$ . We therefore treated both parameters isotropically. We obtained a typical value for the hole mobility,  $\mu = 10 \pm 3 \text{ cm}^2/(\text{V s})$ .<sup>3,22,23,63</sup> For the effective-hole-mass parameter the best fit resulted in  $m_h/m_0 = 1.40 \pm 0.33$ . This value may seem surprising as the value of  $m_h/m_0 = 0.8$ , given in Ref. 25, is often adopted.<sup>22,23</sup> However, the value given in Ref. 25 was taken as the average of

TABLE III. Best-fit values from the IRSE data regression analysis for the broadening values of the TO-phonon modes, LPP modes, and plasmon modes in the long-wavelength limit. The error limits, which correspond to 90% reliability, are given in parentheses.

Sample	$\gamma_{\text{TO},\perp} \equiv \gamma_{E_1(\text{TO})}$ ( $\text{cm}^{-1}$ )	$\tilde{\gamma}_{\text{LO},1\perp}$ ( $\text{cm}^{-1}$ )	$\tilde{\gamma}_{\text{LO},2\perp}$ ( $\text{cm}^{-1}$ )	$\gamma_{p,\perp}$ ( $\text{cm}^{-1}$ )	$\gamma_{\text{TO},\parallel} \equiv \gamma_{A_1(\text{TO})}$ ( $\text{cm}^{-1}$ )	$\tilde{\gamma}_{\text{LO},1\parallel}$ ( $\text{cm}^{-1}$ )	$\tilde{\gamma}_{\text{LO},2\parallel}$ ( $\text{cm}^{-1}$ )	$\gamma_{p,\parallel}$ ( $\text{cm}^{-1}$ )
A	3.8(0.3)	612(128)	6.9(0.4)	600 <sup>a</sup> (127)	4 <sup>b</sup>	642(133)	6.0(0.2)	600 <sup>a</sup> (127)
B	4.2(0.6)	729(147)	16.8(1.2)	709 <sup>a</sup> (144)	4 <sup>b</sup>	803(158)	10.6(0.7)	709 <sup>a</sup> (144)
C	6.2(0.3)	664(92)	15.4(0.6)	640 <sup>a</sup> (90)	4 <sup>b</sup>	666(93)	9.7(0.3)	640 <sup>a</sup> (90)
D	3.9(0.5)	144 <sup>c</sup> (3)	282 <sup>c</sup> (12)	311(11)	4 <sup>b</sup>	144 <sup>c</sup> (3)	282 <sup>c</sup> (12)	335(34)

<sup>a</sup>Isotropically averaged, IRSE data have no sensitivity to anisotropy of the plasmon-mode broadening value.

<sup>b</sup>Assumed values, not varied during data analysis.

<sup>c</sup>Isotropically averaged, IRSE data have no sensitivity to anisotropy of the LPP-mode broadening value.

TABLE IV. Value for the LPP-mode frequencies and the screened plasma frequencies derived from best-fit IRSE values (Tables I and II) by using Eqs. (5) and (8).

Sample	$\tilde{\omega}_{\text{LO},1\perp}$ ( $\text{cm}^{-1}$ )	$\tilde{\omega}_{\text{LO},2\perp}$ ( $\text{cm}^{-1}$ )	$\omega_{p,\perp}$ ( $\text{cm}^{-1}$ )	$\tilde{\omega}_{\text{LO},1\parallel}$ ( $\text{cm}^{-1}$ )	$\tilde{\omega}_{\text{LO},2\parallel}$ ( $\text{cm}^{-1}$ )	$\omega_{p,\parallel}$ ( $\text{cm}^{-1}$ )
A	59.8(2.1)	744.0(0.3)	79.5(2.8)	58.0(2.0)	734.5(0.2) 734.9 <sup>a</sup> (0.4)	79.6(2.8)
B	121.6(11.9)	746.2(2.1)	162(16)	117.9(11.6)	737.6(2.5) 737.7 <sup>a</sup> (0.2)	163(16)
C	74.8(8.6)	740.4(0.9)	99.1(11.5)	71.3(8.2)	733.6(1.0) 735.7 <sup>a</sup> (0.5)	97.7(11.4)
D	464.1(3.2)	1028(10)	852(14)	445.1(4.4) 459.3 <sup>a</sup> (1.5)	1047(17)	871(23)

<sup>a</sup>Obtained from Raman data.

values given in Ref. 26 (estimated from near-band-gap absorption coefficients,  $m_h/m_0 \geq 0.6$ ) and Ref. 27 ( $m_h/m_0 = 1.0$  was assumed there to reasonably fit luminescence band-to-band transition energies to the Burstein shift in  $n$ -type  $\alpha$ -GaN), and the effective-mass value of  $0.8m_0$  may have large error bars. A value of  $m_h/m_0 \approx 2.2 \pm 0.2$  was recently determined by Im *et al.*<sup>29</sup> from time-resolved photoluminescence experiments combined with absorption data. In view of recent theoretical results (see Sec. I), the valence-band effective-mass parameters are further expected to show strong anisotropy. Steube *et al.*<sup>30</sup> observed  $2P$  excitons associated with the heavy-hole ( $hh$ ), light-hole ( $lh$ ), and split-off-hole ( $sh$ ) uppermost valence-band states in  $\alpha$ -GaN and derived isotropic effective hole masses  $m_{hh}/m_0 = 1.0 \pm 0.1$ ,  $m_{lh}/m_0 = 1.1 \pm 0.2$ , and  $m_{sh}/m_0 = 1.6 \pm 0.5$  for the different valence-band maxima. According to our investigations, the anisotropy of the effective-hole-mass parameters is not larger than our experimental error, i.e., the anisotropy should be less than  $\sim 25\%$ . Crucial for analysis of the energy dependence of the effective mass is the knowledge of the position of the Fermi level within the valence bands. According to Kim *et al.*,<sup>7</sup> the valence bands in  $\alpha$ -GaN are nonparabolic because of the spin-orbit interaction. They calculated energy-dependent effective hole masses and showed, e.g., that  $m_{hh}$  increases from  $0.33m_0$  for holes at the top of the uppermost valence band up to  $\sim 1.75m_0$  for heavy-hole energies of  $\sim 25$  meV.

The high electron concentration in the  $\alpha$ -GaN film of sample *D* causes enormous changes in the entire range of the IRSE spectra compared to the low conductive films of samples *A*, *B*, and *C* (Figs. 1 and 2). The free carriers effectively screen the polar phonon modes of sapphire and  $\alpha$ -GaN. Hence, the spectral features that can be directly attributed to the  $E_1(\text{TO})$  mode and the high-frequency  $A_1$ -LPP mode ( $\tilde{\omega}_{\text{LO},2\parallel}$ ) appear strongly damped. The large dip in  $\Psi$  observed in samples *A*–*C* near  $\tilde{\omega}_{\text{LO},2\parallel} \sim \omega_{\text{LO},\parallel}$  [ $A_1(\text{LO})$ ] nearly vanishes because of  $\tilde{\omega}_{\text{LO},2\parallel} = 1047 \text{ cm}^{-1}$  due to the high free-electron concentration value  $N_e = 1 \times 10^{19} \text{ cm}^{-3}$  within sample *D*. However, a small dip remains near  $\omega_{\text{LO},\parallel}$  in the IRSE spectra [marked by an asterisk in Fig. 3(b)]. A thin depletion layer at the sample surface, where the concentration of the free carriers is considerably lowered, may give rise to this structure. This effect can be explained by Fermi-level pinning at surface states that are localized within the band gap. The resulting band bending causes a surface

carrier-depleted layer. Accordingly, the  $A_1(\text{LO})$  mode is not screened by free carriers within this very thin surface layer. We assumed this depletion layer to be homogeneous and without free-carrier contribution to the  $\alpha$ -GaN dielectric function, i.e., we used Eq. (1) instead of Eq. (9), and we obtained a thickness of about 5 nm. Such depletion layers were observed previously on the top of MOCVD-grown Si-doped  $n$ -type  $\alpha$ -GaN films investigated by IRSE.<sup>35,36</sup> Humlíček, Henn, and Cardona found the same effect earlier in heavily doped  $n$ -type GaAs using far-ir ellipsometry.<sup>64</sup> Subtracting the effect of the depletion layer through the model calculation, no  $A_1(\text{LO})$ -like resonance appears in the IRSE spectra of the highly-Si-doped sample *D*. This behavior is well known from Raman data of materials with large free-carrier concentration due to strong LPP coupling.<sup>17,18</sup> Instead of the  $A_1(\text{LO})$  phonon, two  $A_1$ -LPP modes exist, where the upper mode is usually strongly broadened and difficult to observe by Raman scattering. In the micro-Raman spectrum of sample *D* (Fig. 4) the broadened low-frequency  $A_1$ -LPP mode ( $\tilde{\omega}_{\text{LO},1\parallel}$ ) occurs at  $459 \text{ cm}^{-1}$ , and the  $A_1(\text{LO})$  mode peak is absent. The LPP mode  $\tilde{\omega}_{\text{LO},2\parallel}$  is difficult to observe in the Raman spectrum of sample *D* because according to the IRSE results this branch should occur highly broadened ( $\tilde{\gamma}_{\text{LO},2\parallel} = 282 \text{ cm}^{-1}$ ) at  $1047 \text{ cm}^{-1}$ . Following the same approach as used above for  $p$ -type  $\alpha$ -GaN, we assumed the Hall concentration value ( $N_e = 1 \times 10^{19} \text{ cm}^{-3}$ ) for our data analysis and fitted the electron mobility and effective-mass parameters as well as their anisotropy. We obtained typical values for the electron mobility,  $\mu_{\parallel} = 122 \pm 13 \text{ cm}^2/(\text{V s})$ ,  $\mu_{\perp} = 127 \pm 6 \text{ cm}^2/(\text{V s})$ .<sup>3</sup> For the effective-electron-mass parameters the best fit resulted in  $m_{e\parallel}/m_0 = 0.228 \pm 0.008$  and  $m_{e,\perp}/m_0 = 0.237 \pm 0.006$ . The effective electron mass reveals no significant anisotropy, and the values resemble those obtained by Perlin *et al.*<sup>15</sup>

In order to illustrate the LPP-coupling effects on our model dielectric functions,  $\text{Im}\{\epsilon_{\perp}\}$  and  $\text{Im}\{-1/\epsilon_{\perp}\}$  spectra of all  $\alpha$ -GaN layers are depicted in Fig. 5. The  $E_1(\text{TO})$  resonance appears as a strong peak in the  $\text{Im}\{\epsilon_{\perp}\}$  spectra independent of the free-carrier concentration in the GaN film [Fig. 5(a)]. Similar to the coupling behavior of the  $A_1(\text{LO})$  mode observed by Raman spectroscopy, for high free-carrier concentration (sample *D*) the  $E_1(\text{LO})$  mode is absent and the broad lower and upper  $E_1$ -LPP branches occur in the energy-loss spectrum  $\text{Im}\{-1/\epsilon_{\perp}\}$  [Fig. 5(b)].

Local vibrational modes (LVM's) can provide valuable information on site location and electronic structure of defects or impurities. Neugebauer and Van der Walle studied hydrogen and hydrogen complexes in GaN theoretically.<sup>65</sup> Many authors reported experimental observation of LVM's in GaN.<sup>66-71</sup> The Raman spectrum of sample *C* (Fig. 4) shows three additional features at  $R_1=265\text{ cm}^{-1}$ ,  $R_2=315\text{ cm}^{-1}$ , and  $R_3=658\text{ cm}^{-1}$  that are very close in frequency to structures reported by Kaschner *et al.* from MBE-grown Mg-doped  $\alpha$ -GaN on sapphire.<sup>69</sup> All modes observed by Kaschner *et al.*<sup>69</sup> exhibit  $A_1$  symmetry. Disorder-activated scattering was suggested for the mode at  $315\text{ cm}^{-1}$ . The authors further attributed the modes at  $265$  and  $658\text{ cm}^{-1}$  to LVM's of Mg in GaN. But Limmer *et al.* observed a similar structure near  $670\text{ cm}^{-1}$  in Raman spectra of thin MBE-grown  $\alpha$ -GaN films after ion implantation not only with  $\text{Mg}^+$ , but also with  $\text{Ar}^+$ ,  $\text{P}^+$ ,  $\text{C}^+$ , and  $\text{Ca}^+$  ions.<sup>70</sup> This structure became more pronounced with increasing ion doses. Therefore, Limmer *et al.*<sup>70</sup> assigned vacancy-related defect LVM's as origin of the structure near  $670\text{ cm}^{-1}$ . However, none of these additional modes are observed within our IRSE data of sample *C*, so we did not consider IM's in our data analysis of sample *C*. Likewise, no IM can be detected in samples *A* and *B*. Other than for sample *D*, where additional ir-active features affect the dielectric response, excellent agreement between measured and calculated data is obtained for samples *A-C* without treatment of further low-polar modes. This is important because, as discussed in Sec. II D, ignoring existent IM's would in particular affect the resulting  $\epsilon_{\infty j}$  values and hence influence our free-carrier results.

Three additional ir-active features are observed in the IRSE spectra of sample *D*. The anharmonic  $\epsilon$  model of Eq. (7) with  $k=1$  and  $l=1$  is no longer valid. Figure 3(a) demonstrates how poor the best-fit calculation with  $k=l=1$  would be. Figure 3(b) presents a magnified  $\Psi$  spectrum of sample *D*, where three additional IM's ( $I_\nu$ ,  $\nu=1,2,3$ ) were included within the best-fit calculation. The IM's are assumed to be isotropic. We find only very small TO-LO splitting values  $\delta\omega_\nu^2$  but large broadening values  $\delta\gamma_\nu$ . In fact, the amount of  $\delta\omega_\nu^2$  is indeterminable, and therefore it is assumed  $\delta\omega_\nu^2=0$  throughout. Note that Eq. (11) is then identical with Eq. (5). The following IM frequencies and broadening values are obtained from the best-fit analysis of sample *D*.

$$I_1: \quad \omega_{\text{IM},1}=574\pm 5\text{ cm}^{-1}, \quad \gamma_{\text{IM},1}=59\pm 17\text{ cm}^{-1}, \\ -\delta\gamma_1=8\text{ cm}^{-1},$$

$$I_2: \quad \omega_{\text{IM},2}=746\pm 5\text{ cm}^{-1}, \quad \gamma_{\text{IM},2}=173\pm 17\text{ cm}^{-1}, \\ -\delta\gamma_2=59\text{ cm}^{-1}.$$

$$I_3: \quad \omega_{\text{IM},3}=851\pm 8\text{ cm}^{-1}, \\ \gamma_{\text{IM},3}=125\pm 42\text{ cm}^{-1}, \quad -\delta\gamma_3=16\text{ cm}^{-1}.$$

To our knowledge, only Sun *et al.*<sup>71</sup> reported on additional ir-active modes in  $\alpha$ -GaN in the frequency range below  $1200\text{ cm}^{-1}$ . The strongest feature was observed by Fourier transform infrared grazing-incidence reflectometry near our  $I_3$  mode at  $848\text{ cm}^{-1}$ . But their film grown on  $\alpha\text{-Al}_2\text{O}_3$  by low-pressure MOCVD was much less  $n$ -type conductive

( $N_e=1.9\times 10^{17}\text{ cm}^{-3}$ ) than the film of sample *D* ( $N_e=1\times 10^{19}\text{ cm}^{-3}$ ). Because of the enormous difference in the doping levels of nearly two orders of magnitude, a common origin of the observed structures in both samples seems unlikely. Siegle *et al.*<sup>72</sup> performed second-order Raman experiments on  $200\text{--}400\text{-}\mu\text{m}$ -thick  $\alpha$ -GaN layers deposited on sapphire, and observed a feature at  $855\text{ cm}^{-1}$  that was found to possess  $A_1$ ,  $E_1$ , and  $E_2$  symmetry. The authors tentatively assigned this peak to an acoustic-optical combination band. Due to the high Si concentration, the IRSE feature  $I_1$  may stem from the ir-inactive, but disorder-activated nonpolar  $E_2^{(2)}$  mode that is located at  $570\text{ cm}^{-1}$  in the Raman spectrum. So far, the origin of the  $I_2$  structure is not clear. The high Si concentration in the  $\alpha$ -GaN film may give rise to an ir-active LVM. Defect-correlated effects and intraband transitions cannot be ruled out, either. Furthermore, the spectral positions and the damping parameters of the three additional modes are found not to change significantly at low sample temperatures  $T$  ( $T=40\text{ K}$ ).

We observe that the values  $\epsilon_{\infty j}$  found here range from approximately 4.9 to about 5.4 (See Table I). For the low-conductivity films,  $\epsilon_{\infty j}$  can be determined with small error bars, whereas for high free-carrier concentrations the error bars for  $\epsilon_{\infty j}$  increase. The latter is not surprising because the parameters  $\epsilon_{\infty j}$  account for the "high-frequency" limits when the dielectric model functions are extrapolated to shorter wavelengths than those studied here. If the free-carrier contribution dominates within the narrow spectral range investigated, it is difficult to determine the constant contribution of the reststrahlen range to the band-gap index of refraction. (Note that contributions due to high-energy electronic transitions, which also affect the dispersion below the fundamental band gap, are not considered here.) The  $\epsilon_{\infty j}$  parameters of highly conductive films could be determined with higher precision when a larger spectral range is used for data analysis. We did not include data from shorter wavelengths because of depolarization effects there. Incoherent wave components, which reflect off the backside of the sapphire substrate when the GaN film starts to become sufficiently transparent, complicate accurate data analysis. Device imperfections, such as the finite focal length of the ir optics, hinder adequate correction of the incoherency effects in the transparency region. The increase of  $\epsilon_{\infty j}$  for samples *C* and *D* (see Table I) compared to the nominally undoped samples *A* and *B* may be explained by the well-known redshift and broadening of the  $\alpha$ -GaN fundamental band gap,<sup>73</sup> but also of the higher-energy transitions with increasing free-carrier concentration. Such effects on higher-energy transitions are well known from highly doped Si.<sup>74</sup> The increase and broadening of the impurity- and defect-related electronic transitions, such as those causing the yellow luminescence, for increasing dopant concentration may be invoked here as another reason.<sup>5,75,76</sup>

We note finally that the phonon-mode frequency values determined by IRSE are consistent with those obtained previously by other methods within the usual variation range.<sup>16,77,78</sup> It is worth mentioning that the broadening value  $\tilde{\gamma}_{\text{LO},2\perp}$  of the high-frequency  $E_1$ -LPP mode increases with the free-electron concentration  $N_e$ , whereas the corresponding TO-broadening  $\gamma_{\text{TO},\perp}$  remains constant. This is seen as a consequence of the anharmonicity of the LPP coupling in

$n$ -type  $\alpha$ -GaN, and resembles that observed in  $n$ -type GaAs.<sup>47</sup> For samples  $A$ – $D$  the best-fit broadening values fulfill the condition of Eqs. (3) and (12) for both polarizations ( $j=\parallel,\perp$ ).

## V. SUMMARY

Infrared spectroscopic ellipsometry was used for measurement of the ir-optical response of  $\alpha$ -GaN films deposited on  $\alpha$ -Al<sub>2</sub>O<sub>3</sub> by MBE. A factorized model, which allows for anharmonic coupling of LO phonons with free-carrier plasmons, was employed to determine the  $p$ -type and  $n$ -type effective-mass and carrier-mobility values. We obtained for the parallel and perpendicular effective-electron-mass parameters  $m_{e,\parallel}/m_0=0.228\pm 0.008$  and  $m_{e,\perp}/m_0=0.237\pm 0.006$ , in very good agreement with earlier observations. The effective-hole-mass parameter was determined without substantial anisotropy to within 25% as  $m_h/m_0=1.40\pm 0.33$ . Even for low-doped  $n$ -type  $\alpha$ -GaN films the IRSE data possess enough sensitivity to the electron concentration and mobility parameters. From line-shape analysis of the el-

lipsometry data we further derived lattice phonon frequencies and broadening values as well as the coupled phonon-plasmon parameters. The  $\alpha$ -GaN lattice-mode parameters are in excellent agreement with previous ir reflectometry and Raman studies as well as our Raman investigations. Three additional ir-active modes with small polarity were observed in highly-Si-doped  $\alpha$ -GaN at 574, 746, and 851 cm<sup>-1</sup>. A carrier-depleted surface layer, similar to those reported from heavily doped GaAs, was found in heavily-Si-doped  $\alpha$ -GaN as well.

## ACKNOWLEDGMENTS

The authors acknowledge G. Lippold and U. Teschner for performing Raman measurements. We thank D. W. Thompson for technical support. We thank B. Rheinländer and J. A. Woollam for their continuing interest in this research. We are indebted to J. Humlíček for providing Ref. 49 prior to its publication. The DFG supported part of the work under Grant No. Rh28-3/1. Part of the work was also supported by the NSF under Contract No. DMI-9901510.

\*Permanent address: Fakultät für Physik und Geowissenschaften, Institut für Festkörperoptik Universität Leipzig, 04103 Leipzig, Germany. Email: mschub@physik.uni-leipzig.de

<sup>1</sup>S. Nakamura and G. Fasol, *The Blue Laser Diode* (Springer, Berlin, 1997).

<sup>2</sup>S. J. Pearton, J. C. Zolper, R. J. Shul, and F. Ren, *J. Appl. Phys.* **86**, 1 (1999), and references therein.

<sup>3</sup>J. W. Orton and C. T. Foxon, *Rep. Prog. Phys.* **61**, 1 (1998), and references therein.

<sup>4</sup>P. Y. Yu and M. Cardona, *Fundamentals of Semiconductors* (Springer, Berlin, 1996).

<sup>5</sup>M. Suzuki, T. Uenoyama, and A. Yanase, *Phys. Rev. B* **52**, 8132 (1995).

<sup>6</sup>G. D. Chen, M. Smith, J. Y. Lin, H. X. Jiang, S.-H. Wei, M. Asif Khan, and C. J. Sun, *Appl. Phys. Lett.* **68**, 2784 (1996).

<sup>7</sup>K. Kim, W. R. L. Lambrecht, B. Segall, and M. van Schilfgaarde, *Phys. Rev. B* **56**, 7363 (1997).

<sup>8</sup>B. Jogai, *Solid State Commun.* **107**, 345 (1998).

<sup>9</sup>S. Kamiyama, K. Ohnaka, M. Suzuki, and T. Uenoyama, *Jpn. J. Appl. Phys., Part 2* **34**, L821 (1995).

<sup>10</sup>W. W. Chow, A. Knorr, and S. W. Koch, *Appl. Phys. Lett.* **67**, 754 (1995).

<sup>11</sup>V. Yu. Davydov, N. S. Averkiev, I. N. Goncharuk, D. K. Nelson, I. P. Nikitina, A. S. Polkovnikov, A. N. Smirnov, M. A. Jacobson, and O. K. Semchinova, *J. Appl. Phys.* **82**, 5097 (1997).

<sup>12</sup>G. Mirjalili, T. J. Parker, S. Farjami Shayesteh, M. M. Bülbül, S. R. P. Smith, T. S. Cheng, and C. T. Foxon, *Phys. Rev. B* **57**, 4656 (1998).

<sup>13</sup>S. Tripathy, R. K. Soni, H. Asahi, K. Iwata, R. Kuroiwa, K. Asami, and S. Gonda, *J. Appl. Phys.* **85**, 8386 (1999).

<sup>14</sup>A. S. Barker, Jr. and M. Ilegems, *Phys. Rev. B* **7**, 743 (1973).

<sup>15</sup>P. Perlin, E. Litwin-Staszewska, B. Suchanek, W. Knap, J. Camassel, T. Suski, R. Piotrkowski, I. Grzegory, S. Porowski, E. Kaminska, and J. C. Chervin, *Appl. Phys. Lett.* **68**, 1114 (1996).

<sup>16</sup>T. Kozawa, T. Kachi, H. Kano, Y. Taga, M. Hashimoto, N. Koide, and K. Manabe, *J. Appl. Phys.* **75**, 1098 (1994).

<sup>17</sup>P. Perlin, J. Camassel, W. Knap, T. Taliercio, J. C. Chervin, T.

Suski, I. Grzegory, and S. Porowski, *Appl. Phys. Lett.* **67**, 2524 (1995).

<sup>18</sup>D. Kirillov, H. Lee, and J. S. Harris, Jr., *J. Appl. Phys.* **80**, 4058 (1996).

<sup>19</sup>F. Demangeot, J. Frandon, M. A. Renucci, C. Meny, O. Briot, and R. L. Aulombard, *J. Appl. Phys.* **82**, 1305 (1997).

<sup>20</sup>E. Frayssinet, W. Knap, J. L. Robert, P. Prystawko, M. Leszczynski, T. Suski, P. Wisniewski, E. Litwin-Staszewska, S. Porowski, B. Beaumont, and P. Gibart, *Phys. Status Solidi B* **216**, 91 (1999).

<sup>21</sup>H. Sobotta, H. Neumann, R. Franzheld, and W. Seifert, *Phys. Status Solidi B* **174**, K57 (1992).

<sup>22</sup>G. Popovici, G. Y. Xu, A. Botchkarev, W. Kim, H. Tang, A. Salvador, H. Morkoç, R. Strange, and J. O. White, *J. Appl. Phys.* **82**, 4020 (1997).

<sup>23</sup>F. Demangeot, J. Frandon, M. A. Renucci, N. Grandjean, B. Beaumont, J. Massies, and P. Gibart, *Solid State Commun.* **106**, 491 (1998).

<sup>24</sup>H. Harima, T. Inoue, S. Nakashima, K. Furukawa, and M. Taneya, *Appl. Phys. Lett.* **73**, 2000 (1998).

<sup>25</sup>J. I. Pankove, S. Bloom, and G. Harbeke, *RCA Rev.* **36**, 163 (1975).

<sup>26</sup>B. B. Kosicki, R. J. Powell, and J. C. Burgiel, *Phys. Rev. Lett.* **24**, 1421 (1970).

<sup>27</sup>R. D. Cunningham, R. W. Brander, N. D. Knee, and D. K. Wickenden, *J. Lumin.* **5**, 21 (1972).

<sup>28</sup>C. Merz, M. Kunzer, U. Kaufmann, I. Akasaki, and H. Amano, *Semicond. Sci. Technol.* **11**, 712 (1996).

<sup>29</sup>J. S. Im, A. Moritz, F. Steuber, V. Härle, F. Scholz, and A. Hangleiter, *Appl. Phys. Lett.* **70**, 631 (1997).

<sup>30</sup>M. Steube, K. Reimann, D. Fröhlich, and S. J. Clarke, *Appl. Phys. Lett.* **71**, 948 (1997).

<sup>31</sup>C. Kittel, *Introduction to Solid State Physics* (Wiley, New York, 1976).

<sup>32</sup>D. E. Aspnes, in *Handbook of Optical Constants of Solids*, edited by E. D. Palik (Academic, New York, 1998), Vol. I, p. 89.

<sup>33</sup>T. E. Tiwald, J. A. Woollam, S. Zollner, J. Christiansen, R. B.

- Gregory, T. Wetteroth, and S. R. Wilson, *Phys. Rev. B* **60**, 11 464 (1999).
- <sup>34</sup>M. Schubert, B. Rheinländer, E. Franke, H. Neumann, T. E. Tiwald, J. A. Woollam, J. Hahn, and F. Richter, *Phys. Rev. B* **56**, 13 306 (1997).
- <sup>35</sup>M. Schubert, A. Kasic, T. E. Tiwald, J. Off, B. Kuhn, and F. Scholz, *MRS Internet J. Nitride Semicond. Res.* **4**, 11 (1999).
- <sup>36</sup>M. Schubert, J. A. Woollam, A. Kasic, B. Rheinländer, J. Off, B. Kuhn, and F. Scholz, *Phys. Status Solidi B* **216**, 655 (1999).
- <sup>37</sup>J. Sik, M. Schubert, T. Hofmann, and V. Gottschalch, *MRS Internet J. Nitride Semicond. Res.* **5**, 3 (2000).
- <sup>38</sup>G. E. Jellison, *Thin Solid Films* **313–314**, 33 (1998).
- <sup>39</sup>M. Schubert, *Phys. Rev. B* **53**, 4265 (1996).
- <sup>40</sup>C. M. Herzinger, P. G. Snyder, B. Johs, and J. A. Woollam, *J. Appl. Phys.* **77**, 1715 (1995).
- <sup>41</sup>C. M. Herzinger, H. Yao, P. G. Snyder, F. G. Celii, Y.-C. Kao, B. Johs, and J. A. Woollam, *J. Appl. Phys.* **77**, 4677 (1995).
- <sup>42</sup>R. M. A. Azzam and N. M. Bashara, *Ellipsometry and Polarized Light* (North-Holland, Amsterdam, 1984).
- <sup>43</sup>M. Schubert, T. E. Tiwald, and C. M. Herzinger, *Phys. Rev. B* **61**, 8187 (2000).
- <sup>44</sup>A. S. Barker, Jr. and J. J. Hopfield, *Phys. Rev. A* **135**, A1732 (1964).
- <sup>45</sup>D. W. Berreman and F. C. Unterwald, *Phys. Rev.* **174**, 791 (1968).
- <sup>46</sup>F. Gervais and B. Piriou, *J. Phys. C* **7**, 2374 (1974).
- <sup>47</sup>A. A. Kukharskii, *Solid State Commun.* **13**, 1761 (1973).
- <sup>48</sup>J. Humlíček, *Philos. Mag. B* **70**, 699 (1994).
- <sup>49</sup>J. Humlíček, R. Henn, and M. Cardona, *Phys. Rev. B* **61**, 14 554 (2000).
- <sup>50</sup>C. A. Arguello, D. L. Rousseau, and S. P. S. Porto, *Phys. Rev.* **181**, 1351 (1969).
- <sup>51</sup>I. Gorczyca, N. E. Christensen, E. L. Peltzer y Blancá, and C. O. Rodriguez, *Phys. Rev. B* **51**, 11 936 (1995).
- <sup>52</sup>C. R. Pidgeon, in *Handbook on Semiconductors*, edited by M. Balkanski (North-Holland, Amsterdam, 1980), Vol. 2, pp. 223–328.
- <sup>53</sup>C. M. Wolfe, N. Holonyak, and G. E. Stillmann, *Physical Properties of Semiconductors* (Prentice-Hall, Englewood Cliffs, NJ, 1989).
- <sup>54</sup>R. P. Lowndes, *Phys. Rev. B* **1**, 2754 (1970).
- <sup>55</sup>M. Schubert, *Thin Solid Films* **313–314**, 323 (1998).
- <sup>56</sup>M. Schubert, B. Rheinländer, J. A. Woollam, B. Johs, and C. M. Herzinger, *J. Opt. Soc. Am. A* **13**, 875 (1996).
- <sup>57</sup>W. H. Press, B. P. Flannery, S. A. Teukolsky, and W. T. Vetterling, *Numerical Recipes: The Art of Scientific Computing* (Cambridge University Press, Cambridge, MA, 1988).
- <sup>58</sup>*Guide to Using WVASE32* (Woollam, Lincoln, 1995), pp. 269–281.
- <sup>59</sup>T. E. Tiwald, D. W. Thompson, and J. A. Woollam, *J. Vac. Sci. Technol. B* **16**, 312 (1998).
- <sup>60</sup>One advantage of rotating-polarizer, rotating-compensator ellipsometry is that the atmospheric absorption, in general, does not affect the ellipsometric parameters as long as the atmospheric conditions remain reasonably stable during one full revolution of the polarizer and analyzer. Slow changes are canceled out by the acquisition procedure. However, rapid changes of the atmospheric conditions will affect the data and should be avoided. Ellipsometry dispenses background measurements, which are necessary to suppress the spurious atmospheric absorption structures from reflectance or transmittance data.
- <sup>61</sup>D. W. Berreman, *Phys. Rev.* **130**, 2193 (1963).
- <sup>62</sup>A. Kasic, M. Schubert, B. Kuhn, J. Off, and F. Scholz (unpublished).
- <sup>63</sup>C. Yuan, T. Salagaj, A. Gurary, A. G. Thompson, W. Kroll, R. A. Stall, C.-Y. Hwang, M. Schurman, Y. Li, W. E. Mayo, Y. Lu, S. Krishnankutty, I. K. Shmagin, R. M. Kolbas, and S. J. Pearton, *J. Vac. Sci. Technol. B* **13**, 2075 (1995).
- <sup>64</sup>J. Humlíček, R. Henn, and M. Cardona, *Appl. Phys. Lett.* **69**, 2581 (1996).
- <sup>65</sup>J. Neugebauer and C. Van de Walle, *Phys. Rev. Lett.* **75**, 4452 (1995).
- <sup>66</sup>M. S. Brandt, J. W. Ager III, W. Götz, N. M. Johnson, J. S. Harris, Jr., R. J. Molnar, and T. D. Moustakas, *Phys. Rev. B* **49**, 14 758 (1994).
- <sup>67</sup>W. Götz, N. M. Johnson, D. P. Bour, M. D. McCluskey, and E. E. Haller, *Appl. Phys. Lett.* **69**, 3725 (1996).
- <sup>68</sup>G.-C. Yi and B. W. Wessels, *Appl. Phys. Lett.* **70**, 357 (1997).
- <sup>69</sup>A. Kaschner, H. Siegle, G. Kaczmarczyk, M. Straßburg, A. Hoffmann, C. Thomsen, U. Birkle, S. Einfeldt, and D. Hommel, *Appl. Phys. Lett.* **74**, 3281 (1999).
- <sup>70</sup>W. Limmer, W. Ritter, R. Sauer, B. Mensching, C. Liu, and B. Rauschenbach, *Appl. Phys. Lett.* **72**, 2589 (1998).
- <sup>71</sup>W. H. Sun, K. M. Chen, Z. J. Yang, J. Li, Y. Z. Tong, S. X. Jin, G. Y. Zhang, Q. L. Zhang, and G. G. Qin, *J. Appl. Phys.* **85**, 6430 (1999).
- <sup>72</sup>H. Siegle, G. Kaczmarczyk, L. Filippidis, A. P. Litvinchuk, A. Hoffmann, and C. Thomsen, *Phys. Rev. B* **55**, 7000 (1997).
- <sup>73</sup>A. Cremades, L. Görgens, O. Ambacher, M. Stutzmann, and F. Scholz, *Phys. Rev. B* **61**, 2812 (2000).
- <sup>74</sup>L. Vina and M. Cardona, *Phys. Rev. B* **29**, 6739 (1984).
- <sup>75</sup>E. F. Schubert, I. D. Goepfert, W. Grieshaber, and J. M. Redwing, *Appl. Phys. Lett.* **71**, 921 (1997).
- <sup>76</sup>I.-H. Lee, I.-H. Choi, C. R. Lee, and S. K. Noh, *Appl. Phys. Lett.* **71**, 1359 (1997).
- <sup>77</sup>C. Wetzel, E. E. Haller, H. Amano, and I. Akasaki, *Appl. Phys. Lett.* **68**, 2547 (1996).
- <sup>78</sup>G. Yu, H. Ishikawa, M. Umeno, T. Egawa, J. Watanabe, T. Soga, and T. Jimbo, *Appl. Phys. Lett.* **73**, 1472 (1998).